Earth, Planets and Space

EXPRESS LETTER

Open Access

Seismic observation using distributed acoustic sensing around the Tsugaru Strait at the Japan and Kuril Trenches, northeastern Japan

Satoru Baba[1*], Eiichiro Araki[1], Takashi Yokobiki[1], Kei Kawamata[2], Keisuke Uchiyama[2] and Takuji Yoshizuka[2]

Abstract

As megathrust earthquakes often have source areas in offshore regions, offshore seismic observations are important. However, the detection capability and resolution of offshore earthquake locations are low owing to the small number of permanent offshore seismic stations. Recently, distributed acoustic sensing (DAS) measurements, which use a fiber-optic cable as a high-density strain rate sensor, have been used for seismic observations. To evaluate the detectability of earthquakes using DAS measurements, locate earthquakes near the cable, and derive the empirical relationship between the magnitude and DAS S-wave strain rate amplitude, we conducted DAS measurements for 4 months using an offshore fiber-optic cable in the Tsugaru Strait, where various types of earthquakes were observed. In this observation, some earthquakes with magnitudes smaller than one or not listed in the earthquake catalog by the Japan Meteorological Agency (JMA) were observed. This suggests a high seismic detection capability for DAS measurements near the cable. We located earthquakes in the Tsugaru Strait by manually picking the arrivals of P- and S-waves. The hypocenters of events near the cable were located near those of the JMA catalog at a kilometer resolution; therefore, DAS data have the potential to locate earthquakes near the cable. In this study, an equation related to the maximum S-wave strain rate amplitude, hypocentral distance, and earthquake magnitude was derived. When the hypocentral distance increased by one order, the amplitude of the S-wave strain rate decreased by approximately 1.8 orders. This attenuation was larger than that derived mainly from inland DAS data in previous studies, which may be due to the difference in scattering or intrinsic attenuation between the inland and offshore regions. Using the derived equation, the magnitude of an earthquake can be estimated using the DAS data. We compared the S-wave amplitudes of the DAS strain rate and the acceleration of the permanent inland stations. The relationship between these two amplitudes is comparable to an apparent S-wave velocity of approximately 710 m/s in the sediment.

Keywords Distributed acoustic sensing, Tsugaru Strait, Offshore earthquakes, Magnitude

*Correspondence:
Satoru Baba
babasatoru@jamstec.go.jp
Full list of author information is available at the end of the article

Graphical Abstract

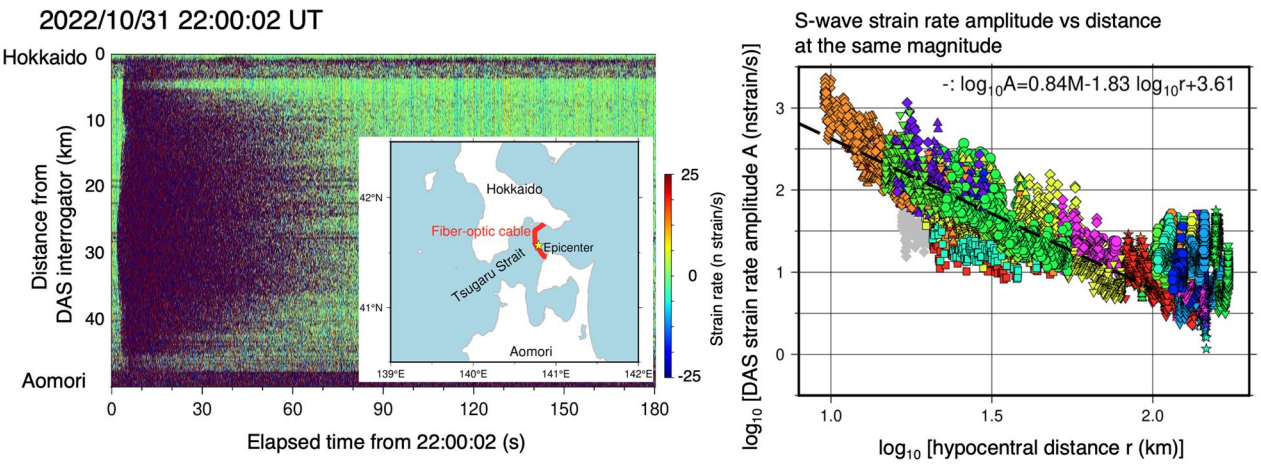

Introduction

Megathrust earthquakes that cause enormous damage often have their source areas in offshore regions. Therefore, offshore seismic observations are important for investigating the tectonic conditions around the plate boundary. Despite the recent installations of seismic observation networks in offshore areas, such as the Dense Oceanfloor Network system for Earthquakes and Tsunamis (Aoi et al. 2020; Kaneda et al. 2015; Kawaguchi et al. 2015) or the Seafloor Observation Network for Earthquakes and Tsunamis along the Japan Trench (Aoi et al. 2020; Kanazawa et al. 2016; Mochizuki et al. 2016; Uehira et al. 2016), the number of permanent seismic stations in offshore areas is smaller than that in inland areas because the installation of offshore networks takes a high cost. Therefore, the detectability and resolution of offshore earthquakes are lower than those of inland earthquakes.

Distributed acoustic sensing (DAS) has recently been used for seismic observations (e.g., Lindsey et al. 2017; Zhan 2019; Ide et al. 2021). DAS conducts strain or strain rate measurements along a fiber-optic cable at intervals of several meters with a high sampling rate (several hundred to one thousand hertz). In DAS measurements, a coherent laser pulse is introduced into a fiber-optic cable, and Rayleigh backscattering occurs at inhomogeneities in the cable. The strain or strain rate can be obtained at each sampling time by measuring the backscattering phase changes. An important feature of DAS is its spatiotemporal density. In addition, already-installed offshore cables can be used for DAS observations; therefore, offshore seismic observations can be realized at a lower cost by DAS than by installing ocean bottom seismometers. Therefore, several studies have recently used DAS for offshore seismic observations (e.g., Lior et al. 2021, 2023; Shinohara et al. 2022; Baba et al. 2023).

The Japan Agency for Marine-Earth Science and Technology and the Electric Power Development Co., Ltd. conducted a DAS observation in the Tsugaru Strait using an offshore fiber-optic cable between Hokkaido and Aomori (Fig. 1). The Tsugaru Strait is located in a subduction zone where the Pacific Plate is subducted beneath the North American Plate in the Japan Trench. Around the Tsugaru Strait, there have been intraslab or interplate earthquakes along the Japan Trench, shallow earthquakes in the Tsugaru Strait and southern Hokkaido, and shallow offshore earthquakes in the Sea of Japan (Additional file 1: Fig. S1). Thus, signals from various earthquake types can be recorded through observations in the Tsugaru Strait.

DAS is a relatively novel technology for seismic observations. Therefore, we first evaluated the detectability of earthquakes using DAS observations in the Tsugaru Strait. We then located earthquakes in the Tsugaru Strait and compared their results with those of an earthquake catalog by the Japan Meteorological Agency (JMA), which is constructed mainly using permanent seismic networks. To construct an earthquake monitoring system using DAS data, the magnitude estimation of earthquakes, as well as detection and location of events, is desired. To estimate magnitudes using only DAS data or a combination of DAS and seismic networks, the relationship between the DAS strain rate and acceleration amplitudes, or the relationship between magnitudes and DAS strain rate amplitudes, should be evaluated. Although Lior et al. (2023) constructed a method of magnitude estimation and a ground motion prediction system

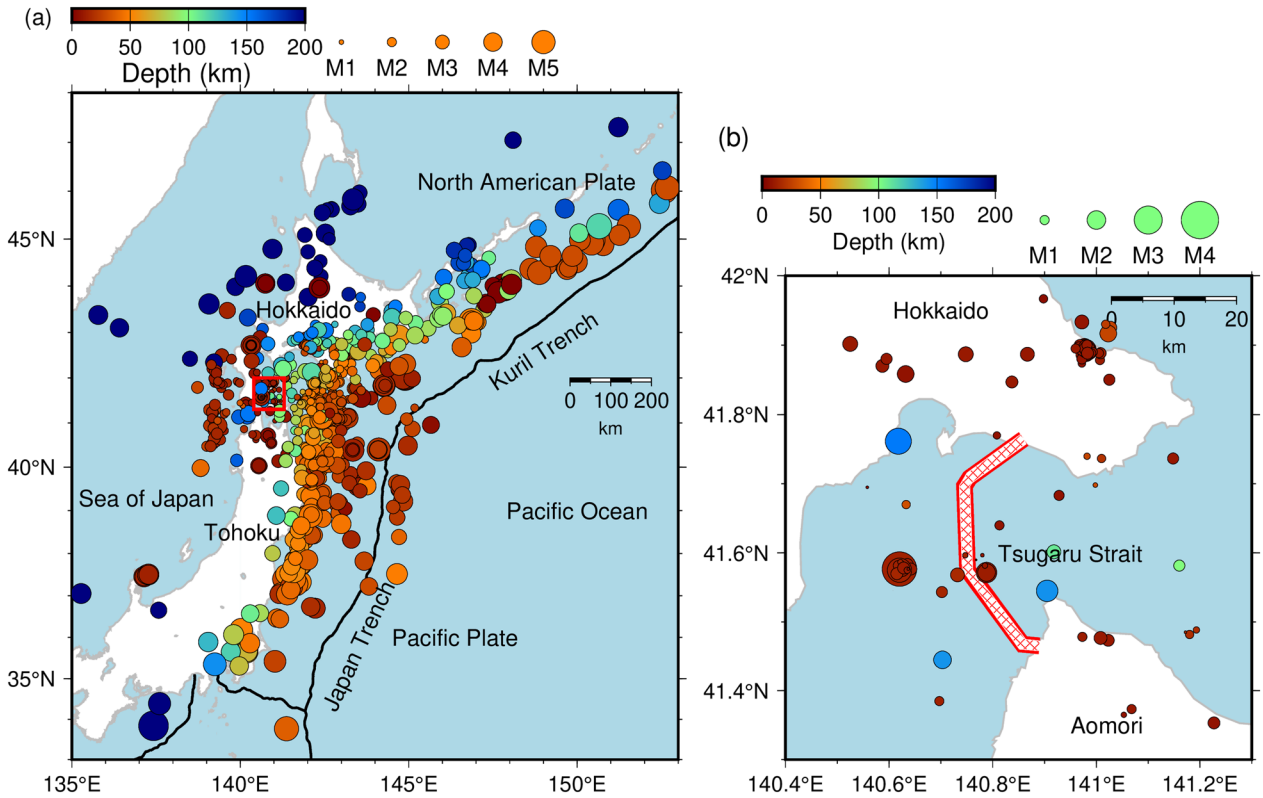

Fig. 1 Distribution of epicenters of earthquakes detected by distributed acoustic sensing (DAS) measurement and listed in the Japan Meteorological Agency (JMA) earthquake catalog. **a** Earthquakes around Japan and **b** zoomed up around Tsugaru Strait shown by the red rectangle in **a**. Black lines are trenches. The fiber-optic cable used for DAS measurement exists in the zone with red hatching

using DAS, the assumption of a stress drop is required. Yin et al. (2023) derived an equation for the relationship between strain rate amplitude, hypocentral distance, and magnitude mainly using inland DAS data. However, the relationship for offshore DAS data has not yet been clarified well. In this study, we derived empirical equations for this relationship using an offshore fiber-optic cable.

Observation of earthquakes around the Tsugaru Strait by DAS

Data

For DAS measurement, we used a fiber-optic cable that connects Hokkaido and Aomori (Fig. 1b). DAS measurement was conducted using a model by AP Sensing (N5226A). An interrogator was placed in Hokkaido. We conducted DAS observation from October 11, 2022, to February 8, 2023. The sampling rate, sensor spacing, and gauge length of the raw data were 500 Hz, 5.1 m, and 40.8 m, respectively. We decimated the raw data to 100 Hz sampling and stacked 10 channels. The decimated and stacked data were prepared at intervals of 30 channels (approximately 150 m). We routinely created spatiotemporal plots of the strain rate by using the decimated and stacked data (Fig. 2).

Earthquakes detected by DAS

We visually checked time–distance plots of the DAS strain rate data at the frequency range of 2–10 Hz (examples are shown in Fig. 2) and listed the earthquake signals, because visual inspection is a more realistic way to find events with low signal-to-noise ratios (Additional file 1: Text S1 and Figs. S2–S4). Next, we searched for the corresponding earthquakes listed in the JMA catalog by checking the time of the events, amplitude distribution, and whether the arrival time order and direction to the hypocenter were consistent with the shape of the cable. We identified 874 earthquakes that corresponded to events in the JMA catalog (Fig. 1a).

In the Tsugaru Strait near the cable, we observed 16 small earthquakes with JMA magnitudes (M_j) smaller than 1. The least M_j was 0.2 (Additional file 1: Fig. S5a). In addition, some events not listed in the JMA catalog were observed (an example is shown in Additional file 1: Fig. S5b). These events were characterized by the fast arrival of seismic waves and their large amplitudes

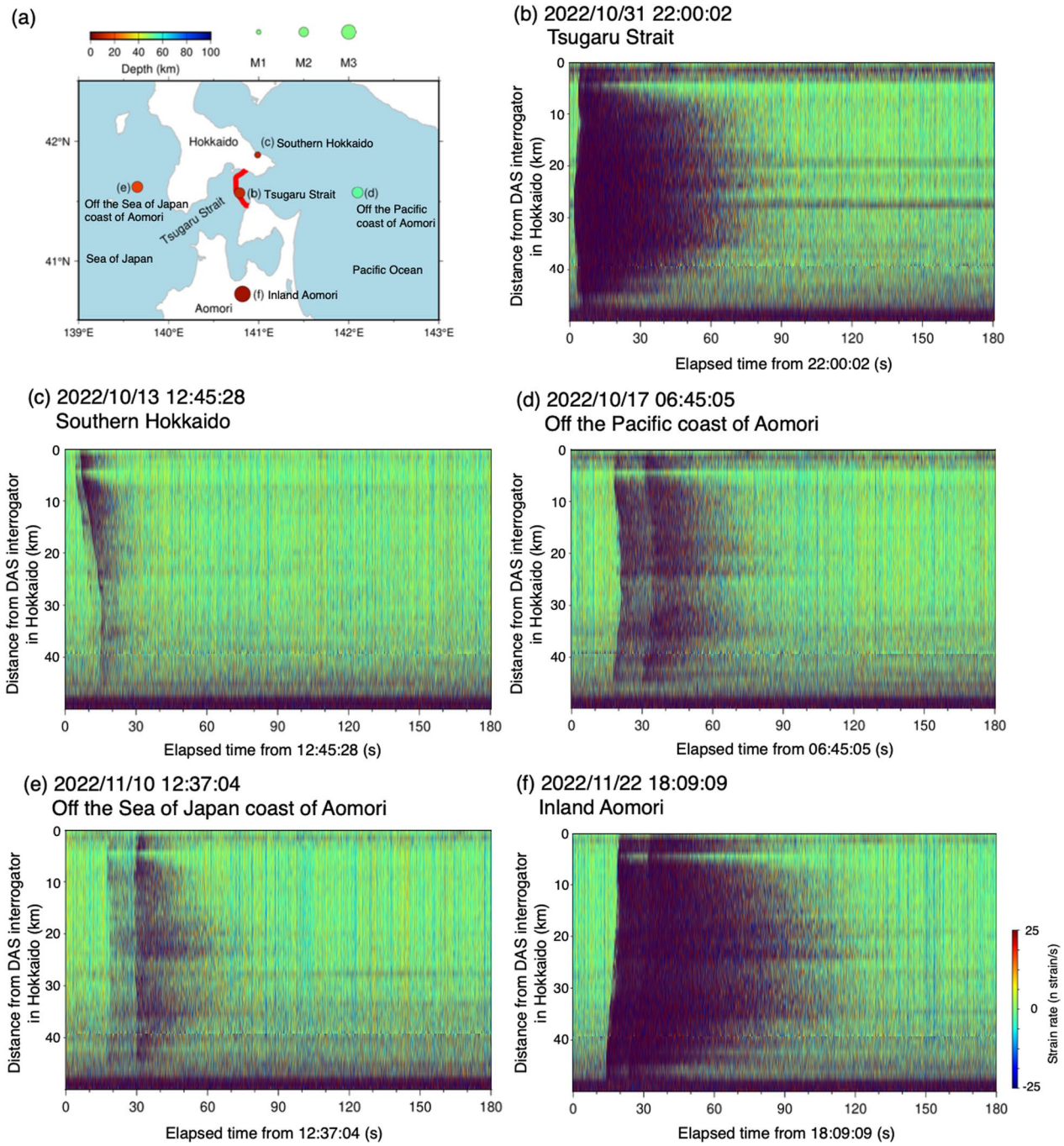

Fig. 2 Examples of earthquake signals recorded by DAS measurement. **a** Map of earthquakes shown in **b**–**f**. The red line represents the fiber-optic cable. **b**–**f** Time–distance plot of strain rate data from DAS measurement at the frequency range of 2–10 Hz when an earthquake occurred. Hypocenters, origin times in UT, and magnitudes of earthquakes are based on the JMA earthquake catalog

inside the Tsugaru Strait. In addition, amplitudes were recorded over a limited channel range. These events can be small earthquakes with $M_j < 1$ in the strait and may not have been detected or located by the JMA because their signals were too small or not recorded in permanent inland networks. It suggests a high seismic detection capability of DAS measurement near the cable. 12 low-frequency earthquakes listed in the JMA catalog that occurred around the Tsugaru Strait were also observed (Additional file 1: Fig. S5c). The

characteristic of signals of low-frequency earthquakes is unclear P-wave arrivals.

Outside the Tsugaru Strait, earthquakes with $M_j > 1$ and $M_j > 2$ were reliably observed within radii of 50 and 200 km from the cable, respectively. Some events with M_j 1–2 were also observed within radius of 50–200 km. At distances greater than 200 km from the cable, only earthquakes with $M_j > 3$ were observed. The largest magnitude event observed in this study around Japan was 6.4 on November 14, 2022, 08:08:25 UT, in the southeast of the Kii Peninsula (Additional file 1: Fig. S5d). At the low frequency band (0.01–0.1 Hz), the signals of the Turkey–Syria earthquake with a magnitude of 7.8 on February 6, 2023, 01:17:34 UT (earthquake catalog by United States Geological Survey, https://earthquake.usgs.gov/earthquakes/search/), were observed (Additional file 1: Fig. S5e). Thus, DAS can observe large teleseismic events as well as local earthquakes near the cable and potentially observe various seismic events.

In the Tsugaru Strait and southern Hokkaido, the depths of most events were approximately 10 km, and the magnitudes were smaller than three (Fig. 1b). For events in the Tsugaru Strait, seismic waves first arrived at the channels inside the strait and propagated northward and southward to the coasts (Fig. 2b). For events in southern Hokkaido, seismic waves propagated from the northern coast. Prominent P- and S-waves and amplitude attenuations were recorded (Fig. 2c).

Nearly half of the observed events were intraslab or interplate earthquakes that occurred along the Japan Trench. The depth of these earthquakes varied from 10 to 150 km because the depth increased owing to plate subduction from the trench axis. For events off the Pacific coast of Aomori, which are intraslab or interplate earthquakes, the arrival time was faster on both sides of the cable and later in the Tsugaru Strait, where the cable sticks out to the west (Fig. 2d). Intraslab or interplate earthquakes along the Kuril Trench or outerrise earthquakes along the Japan and Kuril Trenches with $M_j >$ 3 were also observed.

Shallow events (approximately 10 km) off the Sea of Japan coast of Aomori and southern Hokkaido were also observed. The arrival time variation of these events was similar, although the cable sticks out to the west inside the Tsugaru Strait (Fig. 2e). This suggests that the seismic wave velocity inside the Tsugaru Strait is lower than that near the coast. Inland events in Aomori were also observed. The depth of these events was also approximately 10 km, and the seismic waves propagated from the southern coast (Fig. 2f).

There are 128 events with seismic waves propagating from the northern side and not listed in the JMA catalog (Additional file 1: Fig. S5f). These events always occurred at approximately 02:30 UT once or twice a day, five to seven days a week. This was attributed to the blasting of a mine in the southern Hokkaido. Other signals not listed in the JMA catalog (an example is shown in Additional file 1: Fig. S5b) were small magnitude regular earthquakes or low-frequency earthquakes that were missed by the catalog or small amplitude signals from distant earthquakes that were difficult to identify from the JMA catalog.

Location of earthquakes around the Tsugaru strait by DAS

Determination of the position of DAS channels

To locate earthquakes, determining the position of each channel is necessary. First, we searched for the positions of the bending points of the cable and the intersection points of the coasts and the cable from the Marine Domains Awareness Situational Indication Linkage (Umishiru, https://www.msil.go.jp/msil/Htm/main.html?Lang=1). The cable elevation was determined using seafloor topography data from the Japan Oceanographic Data Center (https://www.jodc.go.jp/jodcweb/index.html).

Then, we determined the DAS channel numbers corresponding to the coastlines by checking the spatial variation in the DAS strain rate waveform before stacking without earthquake signals. For the northern coast, the amplitude of the DAS strain rate at the frequency range of 0.05–10 Hz is generally large for the offshore side channels from channel number 154 (Additional file 1: Fig. S6a). Ocean waves can cause large amplitudes in the offshore areas. We determined the channel number at the northern coastline as 154. The variation in the DAS strain-rate amplitudes on the southern coast was smaller than that on the northern coast, because the shallow sea stretches for a distance from the coast. However, waveforms at the frequency range of 10–40 Hz on a day when ocean waves and wind are relatively strong sometimes vary owing to the waves crashing onto the shore. The characteristics of the waveforms often change at channel number 9167 (Additional file 1: Fig. S6b). Therefore, we determined the channel number at the southern coastline as 9167. We then estimated the channel interval as 4.73 m by dividing the cable length on the map by the channel numbers between the two coastlines. The position of each channel was determined by shifting it 4.73 m along the cable. The channel interval was 7% smaller than the DAS sensor spacing (5.1 m). This may have been caused by the small-scale topography of the seafloor.

Method of location

For the location, we used decimated- and 10-channel-stacked strain rate data at intervals of 30 channels

(approximately 150 m). Approximately 300 channels were used. We applied a bandpass filter to the strain rate waveform at a frequency range of 2–10 Hz, because signals lower than 2 Hz are hidden by microseisms, whereas the noise level is larger in a frequency band higher than 10 Hz. We located eight earthquakes whose P- and S-wave arrivals were visible in DAS plots in the Tsugaru Strait (Fig. 3 and Additional file 1: Table S1). We manually picked the arrivals of the P- and S-waves at each channel. We then located these events using a hypocenter location program, hypomh (Hirata and Matsu'ura 1987), with a one-dimensional structural model of Ueno et al. (2002). The estimation error was also estimated using the hypomh program with phase-picking errors of 0.1 s.

As the model of Ueno et al. (2002) does not always accurately reflect the velocity structure of the Tsugaru Strait, station correction factors were introduced (e.g., Araki et al. 2006; Shinohara et al. 2012). First, we calculated the differences between observed and calculated travel times (O-C times) for each event and channel. At each channel, the median O-C time for all events was calculated. The median O-C time multiplied by -1 at each station was set as the initial station correction factor. The station correction factor was added to the manually picked arrival times for each channel. Using the corrected arrival times, we relocated events using hypomh. We then calculated the O-C times at each event and channel and the median O-C times of all events at each channel again. The updated station correction factor was calculated by subtracting the median O-C time from the initial station correction factor. Using the updated station correction factor, we relocated the events using hypomh. These processes were iterated until the root-mean-square of O-C time did not change significantly. The final station correction factors are shown in Additional file 1: Fig. S7.

Results

For all events, the difference between the epicenters located using DAS data and those by the JMA catalog was less than 0.1° (Fig. 3 and Additional file 1: Table S1).

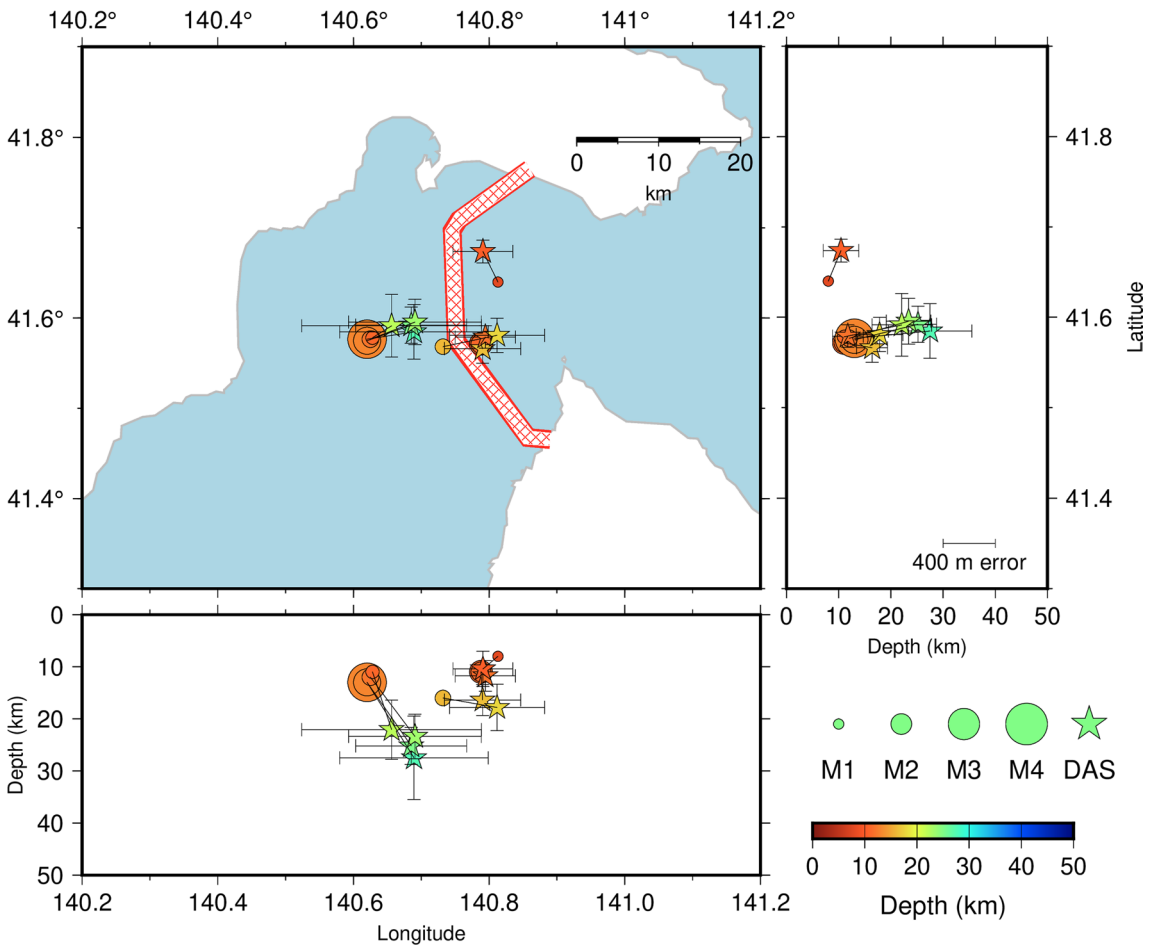

Fig. 3 Earthquake locations determined by DAS data (stars) and JMA (circles). Black lines connect the corresponding events. The fiber-optic cable is shown in Fig. 1b

The events that occurred inside the southern corner of the cable (events #1 and #2 in Additional file 1: Table S1) were located particularly close to the hypocenters in the JMA catalog (epicenter difference was less than 0.01°). This suggests that earthquakes can be located using DAS data only if a cable surrounds the epicenter in multiple directions. The events that occurred west of the cable were located closer to the cable and deeper than the hypocenters in the JMA catalog. The azimuth coverage of the DAS channels is biased to the eastern side of the hypocenters; therefore, a tradeoff exists between the distance from the cable and depth. In general, the error bar is larger in the east–west direction than that in the north–south direction because the cable extends in the north–south direction, and the azimuth coverage of the cable is better in this direction. In addition, the error bars of the events west of the cable were larger because all the DAS channels are distributed to the east relative to the epicenter, and the azimuth coverage of the DAS channels is worse.

The assumed velocity structure was an average one-dimensional seismic velocity structure across Japan and does not necessarily reflect the structure of the Tsugaru Strait. To locate earthquakes with a higher resolution, an investigation of the seismic velocity structure in the Tsugaru Strait and locating earthquakes using the structure can be effective.

Discussion of DAS amplitudes

Site calibration

Most part of the fiber-optic cable used in this study is installed on soft sediments. Therefore, the amplitudes of the seismic waves can be amplified, and the amplification varies by channels. In addition, the coupling between the fiber-optic cable and the ground also varies by channel. As the local geological and instrumental conditions affect the amplitude of the DAS strain rate, we calibrated the site amplification factors.

We estimated the relative site amplification factors of the DAS channels at 2–10 Hz using the method described by Yabe et al. (2019). For the calibration, we used 64 earthquakes with prominent P- and S-wave arrivals in the DAS plots and epicentral distances at the central channel of the cable smaller than 130 km (Fig. 4a and Additional file 1: Table S2). The maximum S-wave amplitude was measured in the time window from 2 s before to 60 s after the calculated S-wave arrival time at each channel, because the duration of signals is ~ 1 min even for the longest cases in targeted events. If the ratio of the maximum amplitude of the S-wave to that of 2–30 s before the P-wave arrival is smaller than two at a channel, the amplitude of this earthquake at this channel was not used in the following procedures due to a low signal-to-noise ratio. The S-wave arrival time was calculated by hypomh using the hypocenters located by the JMA and the one-dimensional structural model of Ueno et al. (2002). The maximum S-wave amplitude of the i-th earthquake at the j-th channel (A_{ij}) is expressed by the following relationship:

$$\log(A_{ij}) = \log(S_i) - \log\left(\sqrt{4\pi}L_{ij}\right) - \alpha L_{ij} + \log(C_j) \quad (1)$$

where S_i is the size of the i-th seismic source, L_{ij} is the distance between the hypocenter of the i-th earthquake and the j-th channel, α represents seismic attenuation, and C_j is the site amplification factor. In "Discussion of DAS amplitudes" section, the hypocentral distance was calculated by using the hypocenter from the JMA catalog. The relative site amplification factor was estimated by solving Eq. (1) using the least-squares method. We estimated the site amplification factors at each channel such that the median value was 1.0 (Additional file 1: Fig. S8).

The data quality of the channels with site amplification factors smaller than ~ 0.5 can be poor probably because of the low coupling between the cable and the ground. Therefore, we did not use the channels with a logarithm of the site amplification factor smaller than − 0.3.

Relationship between magnitudes and DAS strain rate amplitudes

We compared the relationship between the hypocentral distance and DAS strain rate amplitudes for each event shown in Fig. 4a and Additional file 1: Table S2. We used the site-corrected maximum S-wave strain rate amplitudes of each channel, using the method described in "Site calibration" section. There was a negative correlation between a logarithm of the hypocentral distance and a logarithm of the maximum S-wave amplitudes for events near the cable, such as those in the Tsugaru Strait and southern Hokkaido (Fig. 4b and Additional file 1: Fig. S9ab). On the contrary, it was difficult to find a correlation for further events (Fig. 4b and Additional file 1: Fig. S9c).

To derive the relationship between the magnitudes and the DAS strain rate amplitudes using various magnitude events, the maximum S-wave amplitudes plotted in Fig. 4b should be calibrated to values of the same magnitude. Therefore, we investigated the relationship between the magnitude and maximum S-wave amplitudes at the same distance. The magnitude was based on the JMA catalog. For events with epicentral distances smaller than 40 km at the central channel of the cable, the strain rate amplitudes at a logarithm of the hypocentral distance (km) of 1.35 (hypocentral distance of 22.4 km) were estimated using the regression line between a logarithm of the hypocentral distance and a

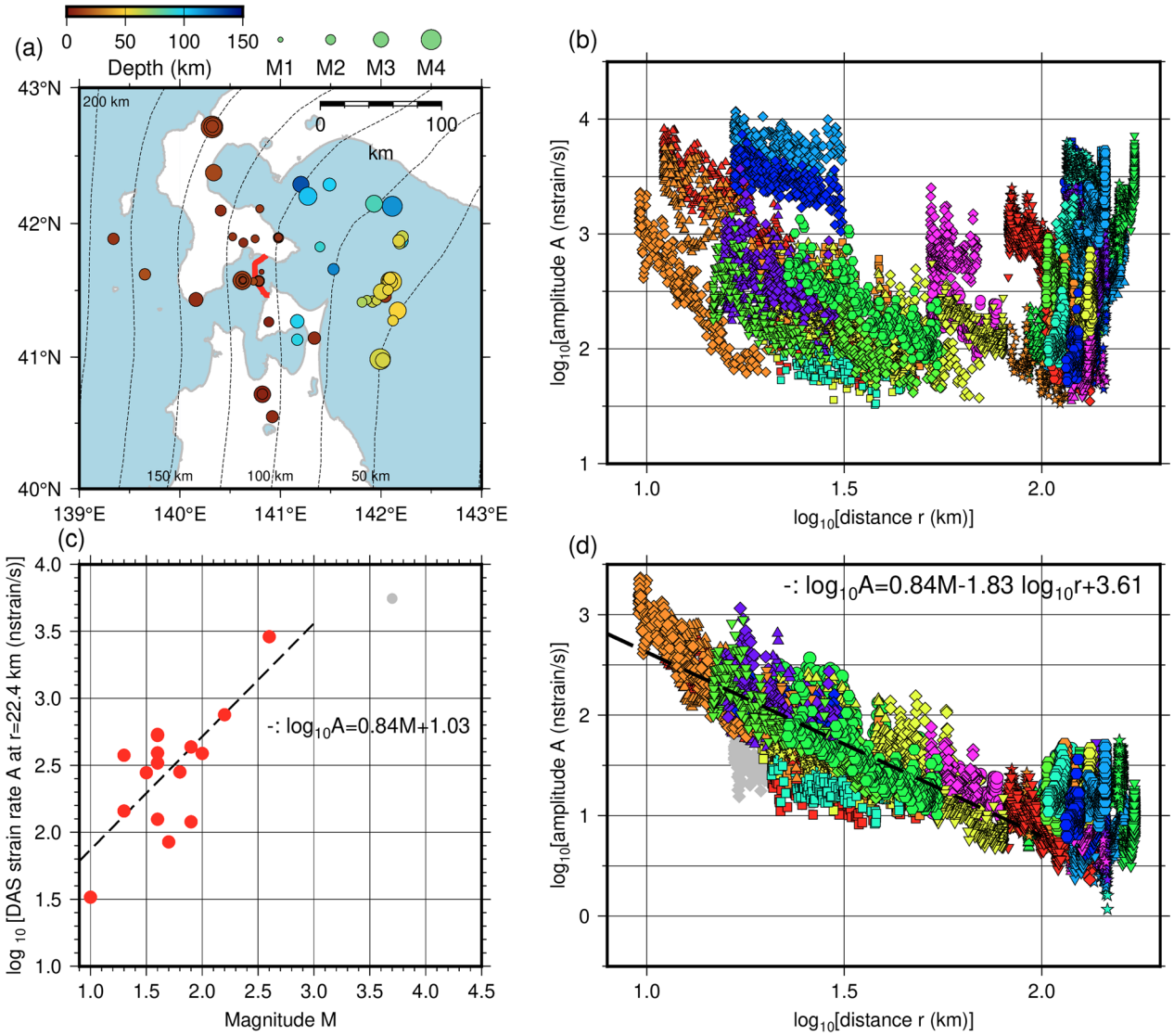

Fig. 4 Relationship between DAS strain rate amplitude, hypocentral distance, and magnitude. **a** Epicenters of earthquakes used for the investigation of the relationship. The red line is the same as in Fig. 1b. Dashed contours indicate the isodepths at the top of the subducting Pacific plate at 25 km intervals (Nakajima and Hasegawa 2006; Kita et al. 2010). **b** Relationship between site-corrected DAS amplitude and hypocentral distance for all events. Different color and shape combinations indicate different events. **c** Relationship between site-corrected strain rate amplitude *A* (nstrain/s) at hypocentral distance of 22.4 km and magnitude *M* for events around the Tsugaru Strait. The dashed line represents the regression line between *A* and *M*. **d** Same as (**b**), but site-corrected strain rate amplitude calibrated to M 1. The dashed line represents the regression line between site-corrected strain rate amplitude *A* (nstrain/s) and hypocentral distance *r* (km). The gray marks in **c** and **d** show the discarded events due to the saturated amplitudes discussed in "Relationship between magnitudes and DAS strain rate amplitudes" section

logarithm of the maximum S-wave amplitudes derived for each event using the least-squares method (Additional file 1: Table S3). We then compared the magnitudes and the strain rate amplitudes at a logarithm of the hypocentral distance (km) of 1.35. A positive correlation was observed between the two values (Fig. 4c). For an event with a magnitude of 3.7, the strain rate amplitudes were smaller for larger magnitudes. This could be caused by amplitude saturation because of phase changes larger than 2π. Therefore, we excluded this event to derive the equations related to the strain rate amplitude. We evaluated the regression line between the strain rate A (nstrain/s) and magnitude M using the least-squares method as follows:

$$\log_{10} A = 0.84M + 1.03. \tag{2}$$

Therefore, as the magnitude increased by one, the strain rate amplitude increased by 0.84 orders. Using this

relationship, we calibrated the maximum S-wave amplitudes to a magnitude of 1 for events in Fig. 4a.

After the calibration of the magnitude, a negative correlation existed between the amplitudes and hypocentral distances smaller than 100 km (Fig. 4d). Therefore, we estimated the regression line between the S-wave strain rate amplitude calibrated to a magnitude of 1 A_1 (nstrain/s) and the hypocentral distance r (km) using the least-squares method as follows:

$$\log_{10}A_1 = -1.83\log_{10}r + 4.46. \tag{3}$$

The relationship between A_1 (nstrain/s) and the S-wave strain rate amplitude before the magnitude calibration A (nstrain/s) is described as follows:

$$\log_{10}A_1 = \log_{10}A - 0.84(M-1). \tag{4}$$

By substituting Eq. (4) into Eq. (3), the relationship among the S-wave strain rate amplitude A (nstrain/s), hypocentral distance r (km), and magnitude M can be obtained as follows:

$$\log_{10}A = 0.84M - 1.83\log_{10}r + 3.61. \tag{5}$$

Using this equation, the magnitudes can be estimated from the DAS strain rate amplitude data.

We also derived an equation between acceleration amplitudes and hypocentral distance using the same procedure and the same earthquakes for the DAS strain rate amplitude. We used accelerometer waveform data with a 100 Hz sampling managed by the Association for the Development of Earthquake Prediction at A.TSRN and A.HRDA (AS-net, Noguchi et al. 2017) near the northern and southern ends of the cable, respectively. We applied a bandpass filter at the frequency range of 2–10 Hz to the acceleration waveforms and measured the maximum S-wave amplitudes of each event (A_{acc}) during the observed seismic wave duration. The acceleration waveforms at A.TSRN and A.HRDA were obtained by rotating the horizontal components to the direction parallel to the cable axial at the northern and southern ends, respectively. The relationship between the S-wave acceleration amplitude A_{acc} (nm/s^2), hypocentral distance r (km), and magnitude M is as follows (Additional file 1: Fig. S10):

$$\log_{10}A_{\mathrm{acc}} = 0.84M - 1.55\log_{10}r + 5.97. \tag{6}$$

The coefficient multiplied by $\log_{10}r$ derived from the DAS strain rate amplitude (1.83) was larger than that derived from the acceleration amplitude (1.55). Although the acceleration is proportional to the strain rate theoretically, the coefficient differs. The small number of acceleration amplitude samples used to derive the equation or the uncertainty of site amplifications at the offshore DAS cable may affect the difference. An investigation using more events is required in future studies.

We compared Eq. (5) with empirical equations related to the magnitudes derived in previous studies. Tsuboi (1954) derived an equation related to magnitude M, maximum displacement amplitude A_{T} [μm], and epicentral distance r [km] from seismograph data set in six cities in Japan, as follows:

$$\log_{10}A_{\mathrm{T}} = M - 1.73\log_{10}r + 0.83. \tag{7}$$

Watanabe (1971) derived an equation related to magnitude M, maximum velocity amplitude A_{W} [cm/s], and hypocentral distance r [km] for small earthquakes ($r < 200$ km), as follows:

$$\log_{10}A_{\mathrm{W}} = 0.85M - 1.73\log_{10}r - 2.50. \tag{8}$$

Yin et al. (2023) derived an equation using the DAS strain rate amplitude A_{Y} [μstrain/s], magnitude M, and hypocentral distance r [km] from DAS data in California, United States of America, as follows:

$$\log_{10}A_{\mathrm{Y}} = 0.690M - 1.588\log_{10}r + K, \tag{9}$$

where K is the site calibration factor.

The coefficient multiplied by M in this study (0.84) is similar to that of Watanabe (1971), smaller than that of Tsuboi (1954), and larger than that of Yin et al. (2023). The differences from the coefficient by Tsuboi (1954) and Yin et al. (2023) may have been caused by the difference in the type of magnitude (JMA magnitude in this study and local or moment magnitude in Yin et al. (2023)) or difference in frequency band used to derive an equation. However, considering the uncertainty of the coefficient in this study (0.84 ± 0.22), the coefficients derived by Tsuboi (1954) and Yin et al. (2023) are in the error bar range. To fix this coefficient with a smaller uncertainty, evaluation using more near events will be required in future work.

The coefficient multiplied by $\log_{10}r$ derived in this study (1.83 ± 0.01) is larger than that in other studies (1.73 in Tsuboi (1954) and Watanabe (1971); 1.588 in Yin et al. (2023)). We conducted DAS observation using offshore fiber-optic cables and mainly marine earthquakes to derive an empirical equation. By contrast, Yin et al. (2023) derived Eq. (9) mainly from inland DAS data using shallow inland earthquakes in California. Tsuboi (1954) and Watanabe (1971) also used inland seismometer data. In offshore areas covered by soft sediments with low seismic velocity and strong structural heterogeneity, scattering and intrinsic attenuation can be stronger than those in inland areas; therefore, the strain rate amplitude around the Tsugaru Strait may be more attenuated than that in inland areas. In fact, the attenuation strength is larger for ocean bottom seismometers than that for inland seismometers in Yabe

et al. (2019) and Yabe et al. (2021). The difference between the coefficient derived in this study and that in other studies may be caused by the difference in attenuation properties between offshore and inland areas.

Following Yin et al. (2023), we also conducted direct fitting (Additional file 1: Text S2), as follows:

$$\log_{10}A = 0.91M - 1.91\log_{10}r + 3.61. \quad (10)$$

The coefficient multiplied by M in Eq. (10) (0.91) is larger than that in Eq. (5) (0.84 ± 0.22) but in the error bar range. The coefficient multiplied by $\log_{10}r$ is also larger in Eq. (10) (1.91) than that in Eq. (5) (1.83). This can be caused by a larger coefficient multiplied by M in Eq. (10). However, regardless of the method, the tendency that the coefficient multiplied by $\log_{10}r$ is larger than that in other studies does not change.

Relationship between DAS strain rate and acceleration amplitudes

To investigate the relationship between the strain rate and acceleration amplitudes, we compared the maximum S-wave amplitudes of DAS strain rate (A_{sr}) with those of acceleration at A.TSRN and A.HRDA (A_{acc}) derived in "Relationship between magnitudes and DAS strain rate amplitudes" section. For each event, we evaluated A_{sr} at the hypocentral distance of A.TSRN and A.HRDA by using the regression line evaluated for each event in "Relationship between magnitudes and DAS strain rate amplitudes" section. We used the earthquakes shown in Fig. 4a with epicentral distances smaller than 40 km at the central channel of the cable. A positive correlation was observed between $\log_{10}(A_{sr})$ and $\log_{10}(A_{acc})$ (Fig. 5). We estimated the regression line between $\log_{10}(A_{sr})$ and $\log_{10}(A_{acc})$ using the least-squares method for all events except the saturated amplitudes discussed in "Relationship between magnitudes and DAS strain rate amplitudes, as follows:"

$$\log_{10}(A_{sr}) = 0.91\log_{10}(A_{acc}) - 2.41. \quad (11)$$

Assuming a plane wave, acceleration A_{acc} can be calculated by multiplying the apparent phase velocity c by the strain rate A_{sr} (e.g., Wang et al. 2018; Lior et al. 2023):

$$A_{acc} = cA_{sr}$$

$$\log_{10}(A_{sr}) = \log_{10}(A_{acc}) - \log_{10}c. \quad (12)$$

We estimated the regression line between $\log_{10}(A_{sr})$ and $\log_{10}(A_{acc})$ by fixing the slope at 1:

$$\log_{10}(A_{sr}) = \log_{10}(A_{acc}) - 2.85. \quad (13)$$

By comparing Eqs. (12) and (13), we obtain $c = 10^{2.85}$ m/s≒710 m/s. The actual velocity dominant in seismic wave propagation along the DAS cable is equal to or slower than ~ 710 m/s. The S-wave in the area of DAS measurement is generally slow and not contradictory with the S-wave velocity in the shallower part of the sediment.

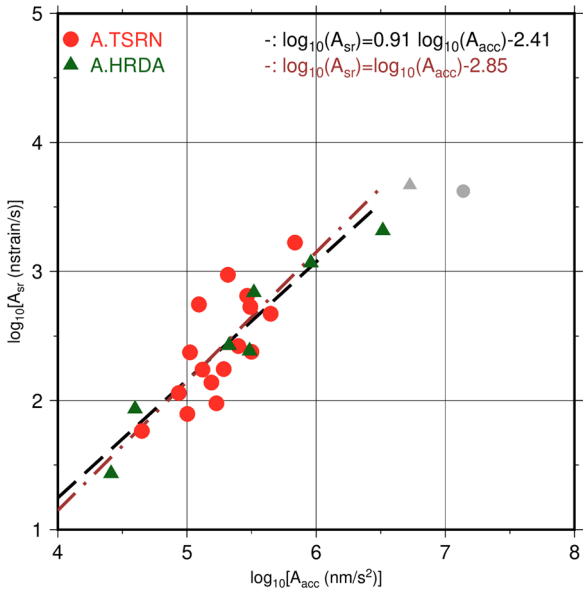

Fig. 5 The relationship between strain rate (A_{sr}) and acceleration (A_{acc}) amplitudes at the stations of A.TSRN (140.8915ºE, 41.7736ºN) and A.HRDA (140.8810ºE, 41.4488ºN). Earthquakes of Fig. 4a with epicentral distances at the central channel of the cable smaller than 40 km were used for the investigation of the relationship. Acceleration waveforms were rotated to the cable direction. Strain rate amplitudes (A_{sr}) at A.TSRN and A.HRDA were estimated from the regression line between DAS strain rate amplitudes and hypocentral distances. Red circles and green triangles show the values of A.TSRN and A.HRDA, respectively. Gray marks show the discarded events due to the saturated amplitudes discussed in Sect. "Relationship between magnitudes and DAS strain rate amplitudes"

In this study, we located earthquakes using only DAS and derived an equation to estimate the magnitude of earthquakes from the strain rate amplitude of DAS. However, the area where the hypocenters can be located is limited by DAS observation alone, with a cable of tens of kilometers. Locating earthquakes over a wider area using DAS and seismograph data together is required. In addition, the wave fields of the strain and velocity amplitudes are different. To estimate the magnitudes, further investigation of the calibration of DAS and seismograph amplitudes is required in future studies.

Conclusions

For seismic observation, we conducted DAS measurement using a fiber-optic cable in the Tsugaru Strait. The least magnitude event was 0.2, and some small earthquakes near the cable not listed in the JMA catalog could be observed. This suggests a high seismic detection

capability for DAS measurement near the cable. By manually picking the P- and S-wave arrivals, we located earthquakes in the Tsugaru Strait using hypomh (Hirata and Matsu'ura 1987). The earthquakes inside the southern corner of the cable were located close to the hypocenters by the JMA catalog. DAS data can be used to locate earthquakes if a cable surrounds the epicenter in multiple directions.

Using DAS data, we derived an equation related to the maximum S-wave strain rate amplitude, hypocentral distance, and magnitude. Using the derived equation, the magnitude of an earthquake can be estimated from the S-wave amplitude of DAS strain rate data. When the hypocentral distance increased by one order, the S-wave strain rate amplitude decreased by approximately 1.8 orders. The S-wave strain rate amplitudes were attenuated more than those in previous studies derived mainly from inland data. This may be caused by the difference in scattering or intrinsic attenuation between the inland regions and the Tsugaru Strait. We also compared the DAS strain rate amplitude with the acceleration amplitude of permanent inland stations. The relationship between these two amplitudes can be explained by an apparent S-wave velocity of ~ 710 m/s. This apparent velocity is not contradictory with S-wave velocity in the shallower part of the sediment.

Abbreviations

DAS Distributed acoustic sensing
JMA Japan Meteorological Agency

Supplementary Information

The online version contains supplementary material available at https://doi.org/10.1186/s40623-024-01975-z.

Additional file 1: Text S1. Trial of STA/LTA method. **Text S2.** Trial of direct fit of the relationship between DAS amplitude, magnitude, and hypocentral distance. **Figure S1.** Distribution of earthquake epicenters listed in the earthquake catalog of the Japan Meteorological Agency (JMA) around the Tsugaru Strait from April 1, 2022, to March, 2023. Dashed contours indicate the isodepths at the top of the subducting Pacific plate at 25 km intervals (Nakajima and Hasegawa 2006; Kita et al. 2010). The red line represents the fiber-optic cable for distributed acoustic sensing (DAS) measurement. **Figure S2.** Distribution of epicenters of earthquakes listed in the JMA earthquake catalog and detected by **a** visual inspection and **b** STA/LTA method. The red line represents the fiber-optic cable. Black lines are trenches. **Figure S3.** Time–distance plot of strain rate data from DAS measurements at 2–10 Hz when events that were found visually but cannot be detected by STA/LTA method occurred. Hypocenters, origin times in UT, and magnitudes of earthquakes were based on the JMA earthquake catalog. **Figure S4.** Time–distance plot of strain rate data from DAS measurements at 2–10 Hz when falsely detected by STA/LTA method. **Figure S5.** Time–distance plot of strain rate data from DAS measurements at 2–10 Hz (**a**–**d**, **f**) or 0.01–0.1 Hz (**e**) when an event occurred. Hypocenters, origin times in UT, and magnitudes of earthquakes were based on the JMA earthquake catalog (**a**, **c**, **d**) or the United States Geological Survey earthquake catalog (**e**). **Figure S6.** Time–distance plot of strain rate waveform **a** near the northern and **b** southern coastlines. **Figure S7.** Station correction factors used for event location based on hypomh (Hirata and Matsu'ura 1987). These factors were added to the observed arrival times of P-wave and S-wave. **Figure S8.** Estimated site amplification factors for each channel. **Figure S9.** Examples of the relationship between the site-corrected DAS amplitude A (nstrain/s) and hypocentral distance r (km) for some events. The dashed lines in **a** and **b** represent the regression lines between A and r. **Figure S10. a** Relationship between the acceleration amplitudes at A.TSRN (140.8915ºE, 41.7736ºN) and A.HRDA (140.8810ºE, 41.4488ºN), managed by the Association for the Development of Earthquake Prediction, and the hypocentral distance for all events. Different combinations of colors and shapes indicate different events. **b** Same as (**a**), but the acceleration amplitude was calibrated to M 1. The dashed line represents the regression line between acceleration amplitude A_{acc} (nm/s^2) and hypocentral distance r (km). **Table S1.** Location of earthquakes analyzed in this study. The lines with JMA and DAS are locations located by JMA and by this study, respectively. **Table S2.** Information in earthquakes used for the discussion of DAS amplitudes in "Discussion of DAS amplitudes" section. Origin times and locations are based on the JMA catalog. **Table S3.** Calculated parameters of the regression line between a logarithm of the hypocentral distance r (km) and a logarithm of the site-corrected DAS amplitude A (nstrain/s) derived for each event using the least-squares method. The relationship between r and A was fitted by $\log_{10}A = a \log_{10}r + b$. List of a and b for each event is shown.

Acknowledgements

We used Generic Mapping Tools (Wessel et al. 2013) and the Seismic Analysis Code (Helffrich et al. 2013) to prepare the figures and the process seismogram data, respectively. We would like to thank Editage (https://www.editage.jp) for English editing. We thank Vice Editor in Chief, Handling Editor, and two reviewers for helpful comments.

Author contributions

SB and EA analyzed the DAS data. SB drafted the manuscript. All authors designed the observations and contributed to data acquisition. All authors read and approved the final version of the manuscript.

Funding

This is a joint research by the Japan Agency for Marine-Earth Science and Technology and the Electric Power Development Co., Ltd., "Joint research and development of offshore monitoring by fiber-optic sensing."

Availability of data and materials

Please contact the corresponding author for the DAS data used in this study. We used the seismograph data managed by the Association for the Development of Earthquake Prediction and the unified earthquake catalog by the Japan Meteorological Agency from the Hi-net webpage (https://hinetwww11.bosai.go.jp/auth/?LANG=en; registration is required). We used United States Geological Survey earthquake catalog (https://earthquake.usgs.gov/earthquakes/search/).

Declarations

Ethics approval and consent to participate

Not applicable.

Consent for publication

Not applicable.

Competing interests

The authors declare no competing interests.

Author details

[1] Japan Agency for Marine-Earth Science and Technology, 2-15, Natsushima-Cho, Yokosuka, Kanagawa 237-0061, Japan. [2] Electric Power Development Co., Ltd, 6-15-1 Chuo-Ku, Tokyo 104-8165, Japan.

Received: 19 October 2023 Accepted: 26 January 2024
Published online: 14 February 2024

References

Aoi S, Asano Y, Kunugi T, Kimura T, Uehira K, Takahashi N, Ueda H, Shiomi K, Matsumoto T, Fujiwara H (2020) MOWLAS: NIED observation network for earthquake, tsunami and volcano. Earth Planets Space 72:126. https://doi.org/10.1186/s40623-020-01250-x

Araki E, Shinohara M, Obana K, Yamada T, Kaneda Y, Kanazawa T, Suyehiro K (2006) Aftershock distribution of the 26 December 2004 Sumatra-Andaman earthquake from ocean bottom seismographic observation. Earth Planets Space 58:113–119. https://doi.org/10.1186/s40623-020-01250-x

Baba S, Araki E, Yamamoto Y, Hori T, Fujie G, Nakamura Y, Yokobiki T, Matsumoto H (2023) Observation of shallow slow earthquakes by distributed acoustic sensing using offshore fiber-optic cable in the Nankai Trough, Southwest Japan. Geophys Res Lett 50:102678. https://doi.org/10.1029/2022GL102678

Helffrich G, Wookey J, Bastow I (2013) The seismic analysis code. Cambridge University Press, Cambridge. https://doi.org/10.1017/CBO9781139547260

Hirata N, Matsu'ura N (1987) Maximum-likelihood estimation of hypocenter with origin time eliminated using nonlinear inversion technique. Phys Earth Planet Inter 47:50–61. https://doi.org/10.1016/0031-9201(87)90066-5

Ide S, Araki E, Matsumoto H (2021) Very broadband strain-rate measurements along a submarine fiber-optic cable off Cape Muroto, Nankai subduction zone. Japan Earth Planets Space 73:63. https://doi.org/10.1186/s40623-021-01385-5

Kanazawa T, Uehira K, Mochizuki M, Shinbo T, Fujimoto H, Noguchi S, Kunugi T, Shiomi K, Aoi S, Matsumoto T, Sekiguchi S, Okada Y (2016) S-net project, cabled observation network for earthquakes and tsunamis. SubOptic. 2016:WE2B-3

Kaneda Y, Kawaguchi K, Araki E, Matsumoto H, Nakamura T, Kamiya S, Ariyoshi K, Hori T, Baba T, Takahashi N (2015) Development and application of an advanced ocean floor network system for megathrust earthquakes and tsunamis. Seafloor Observ. https://doi.org/10.1007/978-3-642-11374-1_25

Kawaguchi K, Kaneko S, Nishida T, Komine T (2015) Construction of the DONET real-time seafloor observatory for earthquakes and tsunami monitoring. Seafloor Observ. https://doi.org/10.1007/978-3-642-11374-1_10

Kita S, Okada T, Hasegawa A, Nakajima J, Matsuzawa T (2010) Anomalous deepening of a seismic belt in the upper-plane of the double seismic zone in the Pacific slab beneath the Hokkaido corner: Possible evidence for thermal shielding caused by subducted forearc crust materials. Earth Planet Sci Lett 290:415–426. https://doi.org/10.1016/j.epsl.2009.12.038

Lindsey NJ, Martin ER, Dreger DS, Freifeld B, Cole S, James SR, Biondi BL, Ajo-Franklin JB (2017) Fiber-optic network observations of earthquake wavefields. Geophys Res Lett 44:11792–11799. https://doi.org/10.1002/2017GL075722

Lior I, Sladen A, Rivet D, Ampuero JP, Hello Y, Becerril C, Martins HF, Lamare P, Jestin C, Tsagkli S, Markou C (2021) On the detection capabilities of underwater distributed acoustic sensing. J Geophys Res Solid Earth 126:e2020JB020925. https://doi.org/10.1029/2020JB020925

Lior I, Rivet D, Ampuero JP, Sladen A, Barrientos S, Sánchez-Olavarria R, Opazo GAV, Prado JAB (2023) Magnitude estimation and ground motion prediction to harness fiber optic distributed acoustic sensing for earthquake early warning. Sci Rep 13:424. https://doi.org/10.1038/s41598-023-27444-3

Mochizuki M, Kanazawa T, Uehira K, Shimbo T, Shiomi K, Kunugi T, Aoi S, Matsumoto T, Sekiguchi S, Yamamoto N, Takahashi N, Shinohara M, Yamada T (2016) S-net project Construction of large scale seafloor observatory network for tsunamis and earthquakes in Japan. AGU Fall Meet. 2016:NH43B-1840

Nakajima J, Hasegawa A (2006) Anomalous low-velocity zone and linear alignment of seismicity along it in the subjected Pacific slab beneath Kanto, Japan: reactivation of subducted fracture zone? Geophys Res Lett 33:L16309. https://doi.org/10.1029/2006GL026773

Noguchi S, Sekine S, Sawada Y, Kasahara K, Sasaki S, Tazawa Y, Yajima H (2017) Earthquake monitoring using dense local seismic network, AS-net, in northern Tohoku, Japan. In: The 16th WCEE, Santiago

Shinohara M, Machida Y, Yamada T, Nakahigashi K, Shinbo T, Mochizuki K, Murai Y, Hino R, Ito Y, Sato T, Shiobara H, Uehira K, Yakiwara H, Obana K, Takahashi N, Kodaira S, Hirata K, Tsushima H, Iwasaki T (2012) Precise aftershock distribution of the 2011 off the Pacific coast of Tohoku Earthquake revealed by an ocean-bottom seismometer network. Earth Planets Space 64:1137–1148. https://doi.org/10.5047/eps.2012.09.003

Shinohara M, Yamada T, Akuhara T, Mochizuki K, Sakai S (2022) Performance of seismic observation by distributed acoustic sensing technology using a seafloor cable off Sanriku, Japan. Front Mar Sci 9:844506. https://doi.org/10.3389/fmars.2022.844506

Tsuboi C (1954) Determination of GUTENBERG-RICHTER's magnitude of earthquakes occurring in and near Japan. Zisin 7:185–193. https://doi.org/10.4294/zisin1948.7.3_185. (**in Japanese with English abstract**)

Uehira K, Kanazawa T, Mochizuki M, Fujimoto H, Noguchi S, Shinbo T, Shiomi K, Kunugi T, Aoi S, Matsumoto T, Sekiguchi S, Okada Y, Shinohara M, Yam-ada T (2016) Outline of seafloor observation network for earthquakes and tsunamis along the Japan Trench (S-net) EGU General Assembly 2016. pp. EGU2016–13832

Ueno H, Hatakeyama S, Aketagawa R, Funasaki J, Hamada N (2002) Improvement of hypocenter determination procedures in the Japan Meteorological Agency. Q J Seismol 65:123–134 (**in Japanese with English abstract**)

Wang HF, Zeng X, Miller DE, Fratta D, Feigl KL, Thurber CH, Mellors RJ (2018) Ground motion response to an ML 4.3 earthquake using co-located distributed acoustic sensing and seismometer arrays. Geophys J Int 213:2020–2036. https://doi.org/10.1093/GJI/GGY102

Watanabe H (1971) Determination of earthquake magnitude at regional distance in and near Japan. Zisin 24:189–200. https://doi.org/10.4294/zisin1948.24.3_189. (**in Japanese with English abstract**)

Wessel P, Smith WHF, Scharroo R, Luis J, Wobbe F (2013) Generic mapping tools: improved version released. Eos (washington DC) 94:409–410. https://doi.org/10.1002/2013EO450001

Yabe S, Tonegawa T, Nakano M (2019) Scaled energy estimation for shallow slow earthquakes. J Geophys Res Solid Earth 124:1507–1519. https://doi.org/10.1029/2018JB016815

Yabe S, Baba S, Tonegawa T, Nakano M, Takemura S (2021) Seismic energy radiation and along-strike heterogeneities of shallow tectonic tremors at the Nankai Trough and Japan Trench. Tectonophysics. https://doi.org/10.1016/j.tecto.2020.228714

Yin J, Zhu W, Li J, Biondi E, Miao Y, Spica ZJ, Viens L, Shinohara M, Ide S, Mochizuki K, Husker AL, Zhan Z (2023) Earthquake magnitude with DAS: a transferable data-based scaling relation. Geophys Res Lett 50:3045. https://doi.org/10.1029/2023GL103045

Zhan Z (2019) Distributed acoustic sensing turns fiber-optic cables into sensitive seismic antennas. Seismol Res Lett 91:1–15. https://doi.org/10.1785/0220190112

Publisher's Note